



1 **Stream laws in tectonic landscape analogue models**

2 Riccardo Reitano¹, Romano Clementucci¹, Ethan M. Conrad², Fabio Corbi³, Riccardo Lanari⁴, Claudio
3 Faccenna^{1,5}, Chiara Bazzucchi¹

4 ¹Department of Science, University of Rome “Roma TRE”, Laboratory of Experimental Tectonics, Rome, Italy

5 ²Department of Geological Sciences, Jackson School of Geosciences, The University of Texas at Austin, Austin, TX, USA

6 ³National Research Council - CNR, Istituto di Geologia Ambientale e Geoingegneria, Italy

7 ⁴Department of Earth Science, University of Florence, Florence, Italy

8 ⁵Lithosphere Dynamics, Helmholtz Centre Potsdam, German Research Centre for Geosciences (GFZ), Potsdam, Germany

9 *Correspondence to:* Riccardo Reitano (r.reitano@gmail.com)

10 *Keywords:* Tectonic Geomorphology, Erosional laws, Analogue modelling.

11 *Keypoints:* Effect of boundary conditions on analogue models using water-saturated granular materials;
12 channelization over more diffusive processes; application of channel power law on analogue models;
13 comparison between natural and analogue geomorphic features.

14 **Abstract**

15 The interplay between tectonics and surface processes defines the evolution of mountain belts.
16 However, correlating these processes through the evolution of natural orogens represents a scientific
17 challenge. Analogue models can be used for analyzing and interpreting the effect of such interaction.
18 We use nine analog models characterized by different combinations of imposed regional slope and
19 rainfall rates to investigate how a small scale orogen evolves in response to tectonics and surface
20 processes. We show how the combination of these parameters control the development of drainage
21 networks and erosional processes. We quantify the different morphological expression of analogue
22 landscapes in terms of a proposed Ae number that accounts for both observables and boundary
23 conditions. We find few differences between analogue models and natural prototypes, in terms of
24 parametrization of the detachment-limited stream power law. We observe a threshold in the
25 development of channelization, modulated by a tradeoff between applied boundary conditions.

26 **1 Introduction**

27 Accurately interpreting the continuous interaction between tectonics and surface processes in mountain
28 belts is one of the main challenges that geologists have faced in the last century. Many limitations exist
29 due to the different spatial and temporal scale depths in which crustal and mantle processes impact the
30 surface. Thus, it is difficult to univocally interpret how different factors interact to build the present-
31 day landscape. Analog models allow for a useful direct control on the evolution of the studied physical
32 process (*e.g.*, Reber et al., 2020), overcoming many of these limitations. Tectonics, erosion, and
33 sedimentation play an integrated role in the evolution of mountain belts with complex and poorly
34 constrained feedbacks. During the last decades modelers analyzed these feedbacks, from the
35 rejuvenation of streams (*e.g.*, Schumm and Parker, 1973; Schumm and Rea, 1995) to the more complex
36 evolution of whole orogenic systems (*e.g.*, Bonnet, 2009; Graveleau and Dominguez, 2008; Guerit et
37 al., 2016; Lague et al., 2003; Tejedor et al., 2017; Viaplana-Muzas et al., 2019; Reitano et al., 2022).
38 However, all the previous analog modeling efforts are based on the robustness of the characterization
39 of material used in the experiments (*e.g.*, Graveleau et al., 2011; Reitano et al., 2020) and on the scaling
40 to natural prototypes (*e.g.*, Graveleau et al., 2011; Paola et al., 2009). While the mechanical, frictional



41 and erosional properties have been characterized empirically and analytically by different authors (*e.g.*,
42 Bonnet and Crave, 2003; Lague et al., 2003; Graveleau et al., 2011; Reitano et al., 2020), the application
43 of erosion laws to analog systems is still a matter of debate. In particular, a definition of the analogue
44 materials response to the applied boundary conditions and an understanding of the variables that modify
45 this response are still missing. These characterizations become even more important considering that a
46 perfect scaling between natural and experimental flow laws is currently missing, limiting the reach of
47 analog studies to insights derived from qualitative process similarity (Paola et al., 2009). In this work
48 we analyze how different boundary conditions affect the evolution of analogue landscapes, in terms of
49 tectonics (imposed regional slope) and climate (rainfall rate). The methodologies implemented here
50 allow us to isolate how different components control features like channelization, morphometrics and
51 incision rates. We are able to define the ranges of external forcings (*i.e.*, rainfall rate and imposed
52 regional slope) in which different morphological features develop (*e.g.*, channels or diffusive
53 processes). Finally, we discuss if and how the erosional parametrization implemented in nature (stream
54 power law) apply to analogue models. Analog models performed in this study represent slow tectonic
55 regions (*e.g.*, very low uplift/erosion rate such as the Anti-Atlas of Morocco; Lanari et al., 2022;
56 Clementucci, 2022), or passive margins such as the Western Ghats escarpment in the western Arabian
57 Sea (Wang and Willett, 2019) and the Southern Australian Escarpment (Godard et al., 2019).

58 2 Experimental Setup, scaling, and erosional laws

59 The analogue material is a granular, water saturated mixture made of 40 wt.% of silica powder, 40 wt.%
60 of glass microbeads and 20 wt.% of PVC powder (Reitano et al., 2020). We fill a $35 \times 30 \times 5$ cm³ box
61 with the material and place it on a reclinable table (Fig. S1). The rainfall system is made of nozzles that
62 provide a dense fog to trigger surface processes. The droplet size in the fog is lower than 100 μ m to
63 avoid rainsplash erosion (*e.g.*, Graveleau et al., 2012). We apply three different rainfall rates on the
64 models: 9, 22, and 70 mm h⁻¹ by controlling the number of implemented nozzles. The angle between
65 the table and the horizontal (*i.e.*, imposed regional slope) is also fixed at three different values, 10°, 15°,
66 and 20°. Both rainfall rate and imposed regional slope are kept constant throughout the experiment. In
67 total, we investigate nine different imposed regional slope-rainfall configurations (Table S1). We use a
68 camera to capture top view digital images of the experiment evolution, and a high-resolution laser
69 scanner to acquire DEMs at defined time-steps. Vertical and horizontal resolution of the laser are 0.07
70 mm and 0.05 mm, respectively.

71 Considering a length scaling factor $L^* = 10^{-5}/10^{-6}$ (1 cm = 1-10 km), a gravitation acceleration scaling
72 factor $g^* = 1$, and a velocity scaling factor $v^* = 10^4-10^5$ (1 cm h⁻¹ = 0.1-1 cm yr⁻¹), the time scaling
73 factor t^* is computed by (Reitano et al. 2020; Reitano et a., 2022)

$$74 \quad t^* = \frac{4L^*}{v^*} \quad \text{Eq. (1)}$$

75 , such that 1 min in the models corresponds to 5 to 50 kyr in nature.

76 The change in elevation (dz) over time (dt) of a point on the surface results from the competition
77 between the rock uplift rate U and the erosion or sedimentation rate E

$$78 \quad \frac{dz}{dt} = U - E \quad \text{Eq. (2)}$$

79 For fluvial networks that show exposed bedrock at the base, the erosion rate is typically expressed as a
80 function of a “detachment-limited stream power law” (*e.g.*, Goren et al., 2014a; Goren et al., 2014b;
81 Howard, 1994; Howard and Kerby, 1983; Tucker and Whipple, 2002)

$$82 \quad E = \kappa Q^m S^n \quad \text{Eq. (3)}$$

83 , where κ is the bedrock erodibility, Q is the channel discharge, S is the channel slope, and m and n are
84 positive exponents accounting for channel geometry, basin hydrology and erosion processes. Since Q
85 is function of drainage area A and rainfall rate P ($Q = A \cdot P$), Eq. (3) can be rewritten as



86 $E = KA^m S^n$ Eq. (4)

87 , where $K = \kappa \cdot P^m$ is controlled by bedrock lithology, incision process and climate (here rainfall rate).
88 Assuming steady-state condition, graded fluvial channels are correctly described by a power
89 relationship between channel slope S and drainage area A (Flint, 1974)

90 $S = k_s A^{-\theta}$ Eq. (5)

91 , where k_s and θ are the channel steepness and the concavity indexes, respectively (e.g. Lanari et al.,
92 2020; Sembroni et al., 2016; Wobus et al., 2006, Kirby and Whipple, 2012; Hack, 1957, 1960).

93 Merging Eq. (4) and (5), and considering that $\theta = m/n$, we can express the result in a logarithmic form
94 $\log_{10} E = n \log_{10} k_s + \log_{10} K$ Eq. (6)

95 Eq. (6) is thus the equation of a line ($y = mx + q$), where n and $\log_{10} K$ are the slope and the intercept of
96 the line, respectively.

97 From the DEMs we compute: (i) topographic metrics such as basin slope and local relief; (ii) channels
98 metrics (k_s and θ) and channel profiles; (iii) eroded volumes, incision rate and erosion maps. We
99 describe the methodologies used for extracting the eroded volumes and incision rates in the
100 Supplementary Information. The above-mentioned analysis are performed using *ad hoc* MATLAB
101 scripts (see data repository) and the TopoToolbox package (Schwanghart and Scherler, 2014).

102 3 Results

103 Table S1 shows a list of the performed experiments, where the first and last two digits of the models'
104 name represent the imposed regional slope and the imposed rainfall rate, respectively (e.g., mod1522,
105 imposed regional slope 15° and rainfall rate 22 mm h⁻¹). These model runs are interpreted highlighting
106 the effect of boundary conditions on the geomorphic models' evolution. Results refer to ten time steps
107 that highlight key stages in the evolution of each model (Supplementary Information), or to the entire
108 experimental run (300 min). Increasing the imposed regional slope and the imposed rainfall rate (from
109 mod1009 to mod2070), the maximum surface slope (MSS) increases systematically from 30° to 80°
110 (between 25th and 75th percentile, Fig. 1a). Mod1009 shows the highest distribution of values.
111 Conversely, the surface slope mode (SSM) decreases for models with the same regional slope but
112 different rainfall rates (e.g., mod1509, mod1522, mod1570), except for mod1009 and mod1022 (Fig.
113 1b), whereas the mode increases for models with the same rainfall rate but different imposed regional
114 slopes (e.g., mod1009, mod1509, mod2009). Models with rainfall rates of 70 mm h⁻¹ show the lowest
115 values in SSM, yet the broadest range of values (between 5° and 15° from mod1070 to mod2070). The
116 decreasing trend in the SSM is also observed in the morphological expression of the model's surface
117 (Figs. S2 and S3). The models with a rainfall rate up to 22 mm h⁻¹ show clear channelization during the
118 final stage of the evolution, while models with rainfall rates equal to 70 mm h⁻¹ shown little to no
119 channelization at final the stage. Only mod2070 develops well-defined channels (branching, narrow
120 channels, incision focused on valleys and into channels). The concavity index ranges from 0.1 to 0.4
121 (between 25th and 75th percentile). Models with the highest rainfall rate typically show the highest
122 concavity values with correspondingly, the highest variability (mod1070, mod1570, mod2070, Fig. 1c).
123 The local relief was extracted using a moving window with a radius of 10 mm. The maximum local
124 relief (MLR) and local relief mode (LRM) show a similar pattern with respect to the surface slope (Fig.
125 1d, e). The MLR increases from mod1009 to mod2070, while the LRM decreases for models having
126 rainfall rate equals to 70 mm h⁻¹ with respect to models having the same imposed regional slope but
127 different rainfall rate. The same information can be deduced by visual inspection of DEMs (Figs. S2,
128 S3).

129 The amount of eroded material ranges from 0.2·10⁶ (mod 1009) to 2.3·10⁶ mm³ (mod 2070) at the last
130 stage of the experiments (Fig. 2a). Both increased rainfall rate (e.g., mod1009, mod1022, mod1070)
131 and increased imposed regional slope (e.g., mod1022, mod1522, mod2022) result in higher amounts of



132 eroded material. All models show an initial phase where the material flux is highest with a later phase
133 of decline (Reitano et al., 2020), tending toward stability. For example, in mod2070, 60 min of
134 experimental time are enough to erode 1.4 mm^3 of material, while in the next 240 min only additional
135 $0.9 \cdot 10^6 \text{ mm}^3$ of material are eroded. This different behavior is most apparent in models with high rainfall
136 rates ($\geq 22 \text{ mm h}^{-1}$) and slopes ($\geq 15^\circ$). The maximum incision rate increases with the imposed regional
137 slope and rainfall rate (Fig. 2b), from $< 5 \text{ mm h}^{-1}$ (mod1009) to ca. 55 mm h^{-1} (mod2070).
138 We extract values for E and k_s of four main channels for each time step and model (40 channels per
139 model, total = 360). Despite the low R^2 values (0.01 – 0.28), n ranges between -0.18 and 0.14 with K
140 values between 0.77 and $23.51 \text{ mm}^{1-2m} \text{ h}^{-1}$. Values of K increase as a function of the slope and rainfall
141 rate, while n does not show a clear trend. On the right hand of Fig. 3, we plot data for models with the
142 same imposed regional slope but different rainfall rates. Models with the same regional slope show a
143 gradually increasing k_s and incision rate in response to increased rainfall rates (Fig. 3b). Interestingly,
144 estimates of K gradually increase in models with imposed regional slope of 10° to 20° (Fig. 3b).

145 4 Discussion

146 4.1 Type of erosion as a function of boundary conditions

147 Our analogue models are controlled exclusively by imposed regional slope and rainfall rate, as no other
148 external forcing is applied (e.g., vertical uplift or horizontal advection of material). Higher rainfall rates
149 (70 mm h^{-1} in this work) tend to inhibit the development of a channelized and branching channel
150 network in favor of more diffusive and mass wasting processes. This trend can be deduced by analyzing
151 the DEMs of mod1070 and mod1570 (Fig. S2), or simply by noting the diffuse nature of erosion under
152 high rainfall conditions (Fig. S3). Mod2070 develop channelization more than mod1070 and mod1570
153 but, similarly, mod1570 show slightly more channelization than mod1070. These observations suggest
154 that the higher the slope, the more effectively a system responds to the high rainfall rates in terms of
155 channelization. Considering the relationship between channelization and boundary conditions, the
156 results of our experiments suggest that low imposed regional slope (mod1009, mod1022) or low rainfall
157 rate with average imposed regional slope (mod1509) result in a channelization characterized by low
158 incision values ($< 25\text{-}30 \text{ mm}$ at final stage). It thus appears that a threshold exists in rainfall rate for the
159 developing of channelization, modulated by the slope over which erosion acts. For example, a rate of
160 70 mm h^{-1} (mod1070 and mod1570) is too high for a proper channel network to develop, while a higher
161 imposed regional slope (mod2070), provide sufficient potential energy to the system to develop
162 channelization (e.g., Burbank and Anderson, 2012). Thus, the tradeoff between imposed regional slope
163 and rainfall rate controls the development of channelization. For higher rainfall rate (mod1070 and
164 mod1570), a sheetlike runoff lowers the model slope homogeneously (Fig. 1b). Furthermore, both the
165 SSM and the LRM drop with respect to models with the same imposed regional slope but lower rainfall
166 rate. From these observations, we argue that at high rainfall rate channelization is subordinate to
167 diffusive processes (controlled by ridge stability) at final stages of model evolution.

168 In landscapes where incision is function of the detachment of particles from the riverbed, the erosion
169 rate is proportional to the shear stress (e.g., Whipple and Tucker, 1999; Yanites et al., 2010). Higher
170 rainfall rate (i.e., higher water discharge) increases the effective shear stress on riverbed (Thoman and
171 Niezgodá, 2008). Since water discharge increases also the channel width (e.g., Shibata and Ito, 2014;
172 C. W. Wobus et al., 2006), for high water discharges (i.e., rainfall rate) the shear stress can distribute
173 over time over wide and flat surfaces instead of focusing in valleys (Lamb et al., 2015 and references
174 therein). At high rainfall rate our models show incipient channelization in the initial stages.
175 Channelization is lost in favor of more diffusive processes during late stages of model evolution. High
176 rainfall rate (i.e., high water discharge) lead to higher sediment supply, that can widen channels



177 (Finnegan et al., 2007; Johnson and Whipple, 2010), eventually erasing their morphological expression.
178 Finally, we must address the erosional threshold defined in the works of Lague et al. (2003) and
179 Graveleau et al. (2011). This threshold must be overcome before significant erosion and transport
180 occurs, and specifically apply to models at low imposed regional slope, which may thus lead to even
181 less channelization. Interestingly, effective channelization does not affect the volume of eroded
182 material, which increases with the imposed regional slope and rainfall rate (*e.g.*, the erosion flux is
183 higher in mod1570 than mod1522 and mod1070). To quantify the relationship between the incision
184 rate, the eroded volume, and imposed regional slope and rainfall rate, we define a dimensionless number
185 for erosion Ae , defined as

$$186 \quad Ae = \frac{I}{V} V_n \frac{S_e}{R} \quad \text{Eq. (7)}$$

187 where I is the incision rate (mm h^{-1}), V is the eroded volume, V_n is the eroded volume normalized with
188 respect to all the models, S_e is the imposed regional slope and R is the applied rainfall rate. We plot the
189 Ae as a function of time (Fig. 2c) and at 300 min (end of the experimental run) over the ratio between
190 imposed regional slope and rainfall rate (S_e/R , Fig. 2d). Nearly every model shows a similar evolution
191 of Ae number in time, except for those with medium to high imposed regional slope and high rainfall
192 rates ($S_e > 15^\circ$, $R = 70 \text{ mm h}^{-1}$, mod1570 and mod2070). The latter experiments attain higher values of
193 Ae number throughout the whole experimental run (even showing a decrease in time). The decrease of
194 Ae for mod1570 and mod2070 is due to the decrease in the volume erosion rate (Fig. 2a). The same
195 decrease affects all the other models, but it is less clear due to the lower Ae numbers. Fig. 1d clearly
196 shows the relationship between the imposed boundary conditions (S_e/R) and their effect on the models'
197 evolution (Ae number). Models tend to align on three straight lines (Fig. 2d), following the rainfall rate.
198 When Ae number is higher than $1 \cdot 10^{-3}$ and S_e/R is lower than 0.5 (dark gray, Fig. 1d), channelization is
199 less important than diffusive processes in controlling the erosion. Models with high rainfall rate
200 (mod1070, mod1570, mod2070) or low rainfall rate and low imposed regional slope (mod1009) show
201 low channelization with respect to the other models. Even if mod2070 and mod1009 show
202 channelization in their DEMs (Fig. S2), the level of incision (Fig. S3) shows that erosion is broadly
203 distributed, and not focused in channels or valleys. When Ae number is lower than $1.5 \cdot 10^{-3}$ and S_e/R is
204 lower than 1 (Fig. 1d, medium light gray), channelization processes are present and are responsible for
205 the erosion of the surface. Still, channels and valleys are wide (ca. 6 cm) with respect to models where
206 Ae number is lower than $1 \cdot 10^{-3}$ and S_e/R is higher than 1 (mod1009, mod1509, mod2009, light gray in
207 Fig. 1d). In these latter cases, the maximum incision rate is lower than 20 mm h^{-1} (Fig. 1b), and the
208 eroded volumes range between 0.1 and $0.75 \cdot 10^6 \text{ mm}^3$.

209 It is then clear that a threshold for developing channelization exists. This threshold is modulated mainly
210 by the rainfall rate, but also by the imposed regional slope. For instance, models with Ae number lower
211 than $1.5 \cdot 10^{-3}$ and S_e/R higher than 0.5, develop channelization. We propose that the Ae number can be
212 used as a threshold parameter to define if and how channelization processes may develop in analogue
213 models.

214 **4.2 Geomorphological metrics in analogue models and natural prototypes**

215 The concavity index θ of the selected channels (for every model) is usually lower than 0.4 (Fig. 1c,
216 values between 25th and 75th percentile). The lower values of θ are related to straight longitudinal
217 channel profiles (Fig. S4) that are established over the course of a model (Duvall, 2004; Reitano et al.,
218 2020; Whipple and Tucker, 1999). Still, θ is comparable between analogue models and natural
219 prototypes (within 0.1, Reitano et al., 2020). However, we do not normalize the steepness index k_s by a
220 reference concavity index (k_{sm}), as usually done in literature (*e.g.*, Cyr et al., 2010; DiBiase et al., 2010;
221 Kirby and Whipple, 2012; Lanari et al., 2020; Tucker and Whipple, 2002). This approach is used so



222 that the steepness index directly reflects channel characteristics, without modifying the data with a
223 normalization parameter.

224 If $n = 1$, there exists a linear relationship between incision rate and k_s - i.e., an increase in the steepness
225 index increases the incision rate and vice versa (Eq. 6). Previous works that computed values of n for
226 different natural landscapes show that n is typically greater than or equals 1 (e.g., DiBiase et al., 2010;
227 Harel et al., 2016; Ouimet et al., 2009), meaning that incision rates are extremely sensitive to variation
228 in the k_s of rivers in active tectonic settings (Kirby and Whipple, 2012). In slow tectonic settings, the
229 incision rates show a lower sensitivity to the steepness index (Olivetti et al., 2016; Clementucci, 2022).
230 For this case, we show that n has values generally lower than 1, even negative (Fig. 3, left plots). Since
231 n is dimensionless, a 1:1 comparison between models and nature is possible. The n results from our
232 analogue models, are closer to estimates of n values from slow tectonic settings compared to active
233 domains, where n is greater than 1 (Figs. 3b and 4; Kirby and Whipple, 2012; Clementucci, 2022).
234 Similar to slow tectonics landscapes in nature, incision rates of analogue models are less sensitive to
235 variations in the steepness index k_s . Moreover, the low R^2 (Fig. 3) testifies a poor relationship between
236 incision rate and k_s ($n < 1$). Nevertheless, we observe a trend in the relationship between incision rate
237 and k_s as a function of the applied rainfall rate (Fig. 3, right panel). For higher rainfall rates, the incision
238 rate increases as expected, but only with a slight increase in the k_s . This consideration supports the fact
239 that the k_s plays a minor role in controlling the incision rate, like slow tectonic natural domains. Note,
240 many works in literature compute values of incision rate and k_s (or k_{sn}) for tectonically active regions.
241 The models presented here are similar to natural prototypes where tectonics is absent or subordinate
242 with respect to surface processes. To show this, we collect values of incision rate and k_{sn} for natural
243 prototypes that show no or almost no active tectonics, and compute values of n and K (Fig. 4). Estimates
244 of n from the analogue models present a good match with data from the selected slow tectonics natural
245 prototypes (Fig. 4), showing values between -0.06 and 0.32 for analogue models (Fig. 3) and -0.12 and
246 0.62 for natural systems (Fig. 4). This relationship is apparent despite the low R^2 value from linear
247 regression of data from analogue and natural cases. Importantly, the difference in the range of n values
248 can be likely decreased by excluding data with a higher uplift rate in the slow tectonic settings (e.g.,
249 granite dominated basins; Clementucci, 2022).

250 Values of K are more difficult to compare between models and nature, due to the complex dimensions
251 that characterize the parameter ($\text{mm}^{1-2m} \text{h}^{-1}$), which require not only the application of a scaling factor,
252 but the definition and comparison of the m variable. Still, it is possible to analyze how the boundary
253 conditions affect K . Because K is mainly function of the lithology and climate (section 2), and we use
254 the same homogenous material for all the models, K only highlights the effect of the rainfall rate. There
255 is a nearly perfect linearity between K and the rainfall rate. For example, from 9 to 22 and from 22 to
256 70 mm h^{-1} , the rainfall rate increases 2.4 and 3.18 times, respectively. This is also apparent for K , with
257 the only exception of the experiment with both moderate imposed slope and rainfall rate (mod1522).
258 Interestingly, there is also a linear relationship between K and the slope. For example, in Fig. 3 when
259 moving from high to low imposed slope. Thus, we speculate that K is not only function of lithologies
260 and climate, but also of the regional slope and, consequently, of the integrated topographic response to
261 tectonic rates, as observed for the natural prototypes (Peifer et al., 2021).

262 5 Conclusions

263 We investigate the role of boundary conditions (imposed regional slope and rainfall rate) on the
264 morphological evolution of nine different analogue models. The models systematically test various
265 configurations of boundary conditions. We analyze how the stream power law used in natural
266 landscapes apply to analogue models. We find that a threshold exists for the development of
267 channelization in terms of boundary conditions (Ae number and S_e/R ratio), and that this threshold is



268 the result of a tradeoff between the imposed regional slope (tectonics) and the rainfall rate (climate).
269 We find that combining imposed regional slope and rainfall rate result in three possible results:
270 • Ae number higher than $1 \cdot 10^{-3}$ and S_e/R lower than 0.5: diffusive processes are dominant with
271 respect to channelization (mod1070, mod1570, mod2070);
272 • Ae number lower than $1.5 \cdot 10^{-3}$ and S_e/R lower than 1: channelization controls the erosion of the
273 surface, with wide channels and valleys (ca. 6 cm);
274 • Ae number lower than $1 \cdot 10^{-3}$ and S_e/R higher than 1 (mod1009, mod1509, mod2009):
275 channelization processes are the main characters in controlling the morphologies of the
276 analogue landscapes.
277 Summarizing, high rainfall rate (70 mm h^{-1}) inhibits the development of channels, but not if coupled
278 with high imposed regional slope (20°). Similarly, low imposed regional slope and low rainfall rate (10°
279 and 9 to 22 mm h^{-1} , respectively) develop channelization characterized by low incision. When looking
280 at the parametrization of the stream power law for erosion, we find that analogue models are described
281 by parameters which values slightly differs from the natural prototypes (*e.g.*, n exponent), and by
282 parameters that are tuned by applied boundary conditions imposed regional slope and rainfall rate (*e.g.*,
283 K constant). Given these findings, we propose that analogue models here presented can and must be
284 used in the interpretation of the interaction between tectonic and surface processes, taking into account
285 the limitations discussed here and the range of applicability of the boundary conditions.

286 **Data Availability**

287 Data have been uploaded open access on GFZ Data Service: [https://dataservices.gfz-](https://dataservices.gfz-potsdam.de/panmetaworks/review/08e477e94c543368eec875408be0db5a4e08ff87ac66f5f03736fcd976b96ac0/)
288 [potsdam.de/panmetaworks/review/08e477e94c543368eec875408be0db5a4e08ff87ac66f5f03736fcd97](https://dataservices.gfz-potsdam.de/panmetaworks/review/08e477e94c543368eec875408be0db5a4e08ff87ac66f5f03736fcd976b96ac0/)
289 [6b96ac0/](https://dataservices.gfz-potsdam.de/panmetaworks/review/08e477e94c543368eec875408be0db5a4e08ff87ac66f5f03736fcd976b96ac0/). These data will receive a doi prior to publication.

290 **Author contribution**

291 RR, RC proposed the original idea. RR, RC and EMC designed the experiments and RR carried them
292 out. RR and FC developed the codes for the model analysis that has been performed by all authors.
293 Interpretation of results, writing, reviewing and editing were performed by all authors.

294 **Acknowledgments**

295 In Figures 2, S2 and S2 we used the perceptually uniform colormap, Roma and Davos, by Fabio
296 Crameri. The grant to the Department of Science, Roma Tre University (MIUR-Italy Dipartimenti di
297 Eccellenza, ARTICOLO 1, COMMI 314-337, LEGGE 232/2016) is gratefully acknowledged.

298 **References**

- 299 Bonnet, S.: Shrinking and splitting of drainage basins in orogenic landscapes from the migration of
300 the main drainage divide, *Nat. Geosci.*, 2(11), 766–771, doi:10.1038/ngeo666, 2009.
- 301 Bonnet, S. and Crave, A.: Landscape response to climate change: Insights from experimental
302 modeling and implications for tectonic versus climatic uplift of topography, *Geol. Soc. Am.*
303 *Bull.*, (2), 123–126, 2003.
- 304 Cyr, A. J., Granger, D. E., Olivetti, V. and Molin, P.: Quantifying rock uplift rates using channel
305 steepness and cosmogenic nuclide – determined erosion rates : Examples from northern and
306 southern Italy | RESEARCH, , 188–198, doi:10.1130/L96.1, 2010.
- 307 DiBiase, R. A., Whipple, K. X., Heimsath, A. M. and Ouimet, W. B.: Landscape form and millennial
308 erosion rates in the San Gabriel Mountains, CA, *Earth Planet. Sci. Lett.*, 289(1–2), 134–144,



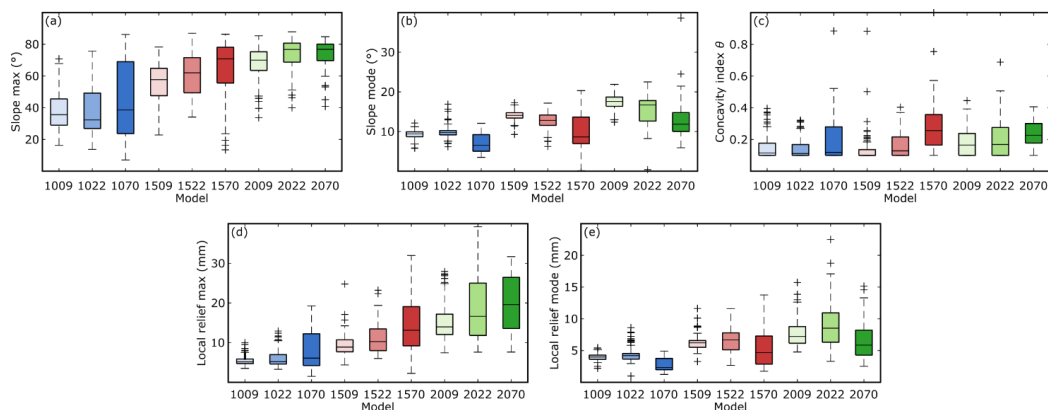
- 309 doi:10.1016/j.epsl.2009.10.036, 2010.
- 310 Duvall, A.: Tectonic and lithologic controls on bedrock channel profiles and processes in coastal
311 California, *J. Geophys. Res.*, 109(F3), 1–18, doi:10.1029/2003jf000086, 2004.
- 312 Finnegan, N. J., Sklar, L. S. and Fuller, T. K.: Interplay of sediment supply, river incision, and
313 channel morphology revealed by the transient evolution of an experimental bedrock channel,
314 *J. Geophys. Res. Earth Surf.*, 112(3), 1–17, doi:10.1029/2006JF000569, 2007.
- 315 Flint, J. J.: Stream Gradient as a Function of Order, Magnitude, and Discharge, *Water Resour. Res.*,
316 10(5), 969–973, 1974.
- 317 Godard, V., Dosseto, A., Fleury, J., Bellier, O. and Siame, L.: Transient landscape dynamics across
318 the Southeastern Australian Escarpment, *Earth Planet. Sci. Lett.*, 506, 397–406,
319 doi:10.1016/j.epsl.2018.11.017, 2019.
- 320 Goren, L., Willett, S. D., Herman, F. and Braun, J.: Coupled numerical-analytical approach to
321 landscape evolution modeling, *Earth Surf. Process. Landforms*, 39(4), 522–545,
322 doi:10.1002/esp.3514, 2014a.
- 323 Goren, L., Fox, M. and Willett, S. D.: *Journal of Geophysical Research : Earth Surface Tectonics*
324 *from fluvial topography using formal linear inversion : Theory and applications to the Inyo*
325 *Mountains , California , 1651–1681, doi:10.1002/2014JF003079. Received, 2014b.*
- 326 Graveleau, F. and Dominguez, S.: Analogue modelling of the interaction between tectonics, erosion
327 and sedimentation in foreland thrust belts, *Comptes Rendus - Geosci.*, 340(5), 324–333,
328 doi:10.1016/j.crte.2008.01.005, 2008.
- 329 Graveleau, F., Hurtrez, J. E., Dominguez, S. and Malavieille, J.: A new experimental material for
330 modeling relief dynamics and interactions between tectonics and surface processes,
331 *Tectonophysics*, 513(1–4), 68–87, doi:10.1016/j.tecto.2011.09.029, 2011.
- 332 Guerit, L., Dominguez, S., Malavieille, J. and Castellort, S.: Deformation of an experimental
333 drainage network in oblique collision, *Tectonophysics*, 693, 210–222,
334 doi:10.1016/j.tecto.2016.04.016, 2016.
- 335 Harel, M. A., Mudd, S. M. and Attal, M.: Global analysis of the stream power law parameters based
336 on worldwide ¹⁰Be denudation rates, *Geomorphology*, 268, 184–196,
337 doi:10.1016/j.geomorph.2016.05.035, 2016.
- 338 Howard, A. D.: A detachment limited model of drainage basin evolution, *Water Resour. Res.*, 30(7),
339 2261–2285, doi:10.1029/94WR00757, 1994.
- 340 Howard, A. D. and Kerby, G.: Channel changes in badlands., *Geol. Soc. Am. Bull.*, 94(6), 739–752,
341 doi:10.1130/0016-7606(1983)94<739:CCIB>2.0.CO;2, 1983.
- 342 Johnson, J. P. L. and Whipple, K. X.: Evaluating the controls of shear stress, sediment supply, alluvial
343 cover, and channel morphology on experimental bedrock incision rate, *J. Geophys. Res. Earth*
344 *Surf.*, 115(F2), doi:10.1029/2009jf001335, 2010.
- 345 Kirby, E. and Whipple, K. X.: Expression of active tectonics in erosional landscapes, *J. Struct. Geol.*,
346 44, 54–75, doi:10.1016/j.jsg.2012.07.009, 2012.
- 347 Lague, D., Crave, A. and Davy, P.: Laboratory experiments simulating the geomorphic response to
348 tectonic uplift, *J. Geophys. Res. Solid Earth*, 108(B1), ETG 3-1-ETG 3-20,
349 doi:10.1029/2002JB001785, 2003.
- 350 Lamb, M. P., Finnegan, N. J., Scheingross, J. S. and Sklar, L. S.: New insights into the mechanics of
351 fluvial bedrock erosion through flume experiments and theory, *Geomorphology*, 244, 33–55,
352 doi:10.1016/j.geomorph.2015.03.003, 2015.
- 353 Lanari, R., Fellin, M. G., Faccenna, C., Balestrieri, M. L., Pazzaglia, F. J., Youbi, N. and Maden, C.:
354 Exhumation and Surface Evolution of the Western High Atlas and Surrounding Regions as
355 Constrained by Low-Temperature Thermochronology, *Tectonics*, 39(3),
356 doi:10.1029/2019TC005562, 2020.
- 357 Lanari, R., Reitano, R., Giachetta, E., Pazzaglia, F. J., Clementucci, R., Faccenna, C. and Fellin, M.
358 G.: Is the Anti-Atlas of Morocco still uplifting?, *J. African Earth Sci.*, 188(January), 104481,
359 doi:10.1016/j.jafrearsci.2022.104481, 2022.
- 360 Olivetti, V., Godard, V. and Bellier, O.: Cenozoic rejuvenation events of Massif Central topography
361 (France): Insights from cosmogenic denudation rates and river profiles, *Earth Planet. Sci.*
362 *Lett.*, 444, 179–191, doi:10.1016/j.epsl.2016.03.049, 2016.
- 363 Ouimet, W. B., Whipple, K. X. and Granger, D. E.: Beyond threshold hillslopes: Channel adjustment



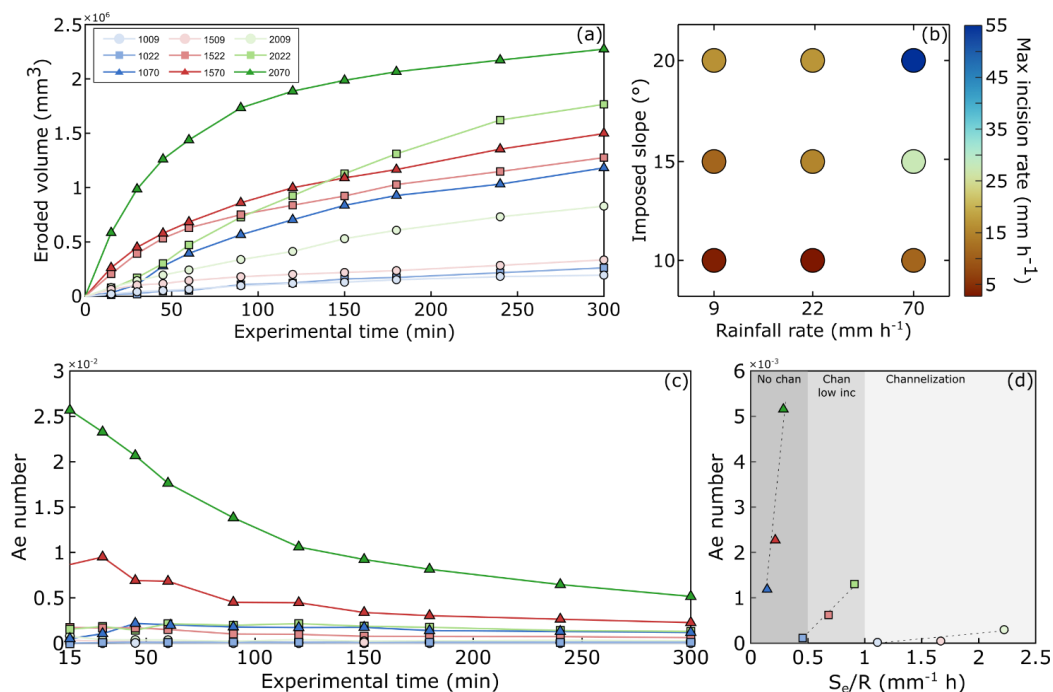
- 364 to base-level fall in tectonically active mountain ranges, *Geology*, 37(7), 579–582,
365 doi:10.1130/G30013A.1, 2009.
- 366 Paola, C., Straub, K., Mohrig, D. and Reinhardt, L.: The “unreasonable effectiveness” of stratigraphic
367 and geomorphic experiments, *Earth-Science Rev.*, 97(1–4), 1–43,
368 doi:10.1016/j.earscirev.2009.05.003, 2009.
- 369 Peifer, D., Persano, C., Hurst, M. D., Bishop, P. and Fabel, D.: Growing topography due to
370 contrasting rock types in a tectonically dead landscape, *Earth Surf. Dyn.*, 9(2), 167–181,
371 doi:10.5194/esurf-9-167-2021, 2021.
- 372 Reber, J. E., Cooke, M. L. and Dooley, T. P.: Earth-Science Reviews What model material to use ? A
373 Review on rock analogs for structural geology and tectonics, *Earth-Science Rev.*,
374 202(September 2019), 103107, doi:10.1016/j.earscirev.2020.103107, 2020.
- 375 Reitano, R., Faccenna, C., Funicello, F., Corbi, F. and Willett, S. D.: Erosional response of granular
376 material in landscape models, *Earth Surf. Dynam.*, 8(4), 973–993, doi:10.5194/esurf-8-973-
377 2020, 2020.
- 378 Reitano, R., Faccenna, C., Funicello, F., Corbi, F., Sternai, P., Willett, S. D., et al. (2022). Sediment
379 recycling and the evolution of analog orogenic wedges. *Tectonics*, 41, e2021TC006951.
380 <https://doi.org/10.1029/2021TC006951>
- 381 Schumm, S. A. and Parker, R. S.: Implications of Complex Response of Drainage Systems for
382 Quaternary Alluvial Stratigraphy, *Nat. Phys. Sci.*, 243, 99–100,
383 <https://doi.org/10.1038/physci243099a0>, 1973.
- 384 Schumm, S. A. and Rea, D. K.: Sediment yields from disturbed earth systems, *Geology*, 23, 391–394,
385 [https://doi.org/10.1130/0091-7613\(1995\)023<0391:syfdes>2.3.co;2](https://doi.org/10.1130/0091-7613(1995)023<0391:syfdes>2.3.co;2), 1995.
- 386 Schwanghart, W. and Scherler, D.: Short Communication: TopoToolbox 2 - MATLAB-based
387 software for topographic analysis and modeling in Earth surface sciences, *Earth Surf. Dyn.*,
388 2(1), 1–7, doi:10.5194/esurf-2-1-2014, 2014.
- 389 Sembroni, A., Molin, P., Pazzaglia, F. J., Faccenna, C. and Abebe, B.: Evolution of continental-scale
390 drainage in response to mantle dynamics and surface processes: An example from the
391 Ethiopian Highlands, *Geomorphology*, 261, 12–29, doi:10.1016/j.geomorph.2016.02.022,
392 2016.
- 393 Shibata, K. and Ito, M.: Relationships of bankfull channel width and discharge parameters for modern
394 fluvial systems in the Japanese Islands, *Geomorphology*, 214, 97–113,
395 doi:10.1016/j.geomorph.2014.03.022, 2014.
- 396 Tejedor, A., Singh, A., Zaliapin, I., Densmore, A. L. and Fofoula-Georgiou, E.: Scale-dependent
397 erosional patterns in steady-state and transient-state landscapes, *Sci. Adv.*, 3(9), 1–8,
398 doi:10.1126/sciadv.1701683, 2017.
- 399 Thoman, R. W. and Niezgod, S. L.: Determining Erodibility, Critical Shear Stress, and Allowable
400 Discharge Estimates for Cohesive Channels: Case Study in the Powder River Basin of
401 Wyoming, *J. Hydraul. Eng.*, 134(12), 1677–1687, doi:10.1061/(ASCE)0733-
402 9429(2008)134:12(1677), 2008.
- 403 Tucker, G. E. and Whipple, K. X.: Topographic outcomes predicted by stream erosion models:
404 Sensitivity analysis and intermodel comparison, *J. Geophys. Res. Solid Earth*, 107(B9), ETG
405 1-1-ETG 1-16, doi:10.1029/2001JB000162, 2002.
- 406 Viaplana-Muzas, M., Babault, J., Dominguez, S., Van Den Driessche, J. and Legrand, X.: Modelling
407 of drainage dynamics influence on sediment routing system in a fold-and-thrust belt, *Basin
408 Res.*, 31(2), 290–310, doi:10.1111/bre.12321, 2019.
- 409 Wang, Y. and Willett, S. D.: The importance of non-vertical flux in the interpretation of detrital
410 cosmogenic nuclide concentrations for basin-wide erosion rates, , (2018), 2018–2019,
411 doi:10.1038/s41586-018-0532-1.0, 2019.
- 412 Whipple, K. X. and Tucker, G. E.: Dynamics of the stream-power river incision model: Implication
413 for height limits of mountain ranges, landscape response timescales, and research needs, *J.
414 Geophys. Res.*, 104(B8), 17661–17674, doi:<https://doi.org/10.1029/1999JB900120>, 1999.
- 415 Wobus, C., Whipple, K. X., Kirby, E., Snyder, N., Johnson, J., Spyropolou, K., Crosby, B. and
416 Sheehan, D.: Tectonics from topography: Procedures, promise, and pitfalls, *Spec. Pap. Geol.
417 Soc. Am.*, 398(September 2016), 55–74, doi:10.1130/2006.2398(04), 2006a.
- 418 Wobus, C. W., Tucker, G. E. and Anderson, R. S.: Self-formed bedrock channels, *Geophys. Res.*



419 Lett., 33(18), 1–6, doi:10.1029/2006GL027182, 2006b.
420 Yanites, B. J., Tucker, G. E., Mueller, K. J., Chen, Y. G., Wilcox, T., Huang, S. Y. and Shi, K. W.:
421 Incision and channel morphology across active structures along the Peikang River, central
422 Taiwan: Implications for the importance of channel width, Bull. Geol. Soc. Am., 122(7–8),
423 1192–1208, doi:10.1130/B30035.1, 2010.
424
425
426
427
428
429
430
431

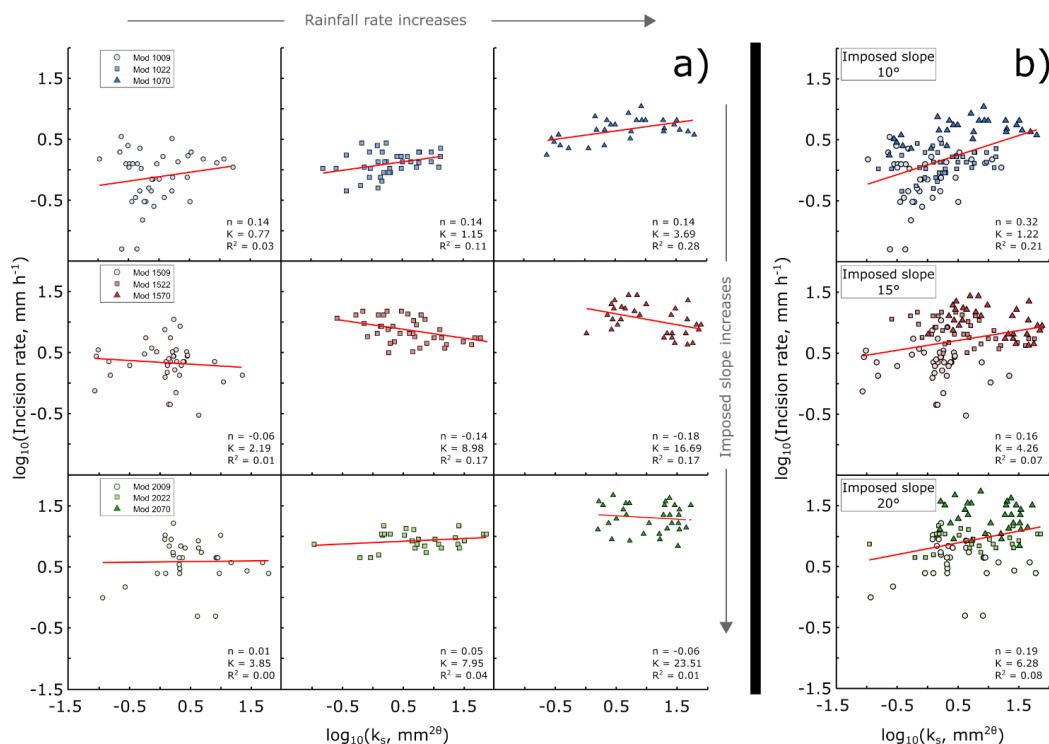


432
433 **Figure 1. Geomorphological and channels metrics of the performed experiments. The black solid**
434 **lines indicate the median, while the bottom and top edges of the colored boxes indicate the 25th**
435 **and 75th percentiles, respectively. The black whiskers outside the boxes cover the data point at**
436 **<25th and >75th percentiles that are not considered outliers, here indicated by black crosses. The**
437 **color saturation in the boxes is related to the applied rainfall rate (less saturated, less rainfall**
438 **rate). The blue, red and green boxes refer to models at 10°, 15° and 20° of imposed slope,**
439 **respectively.**
440

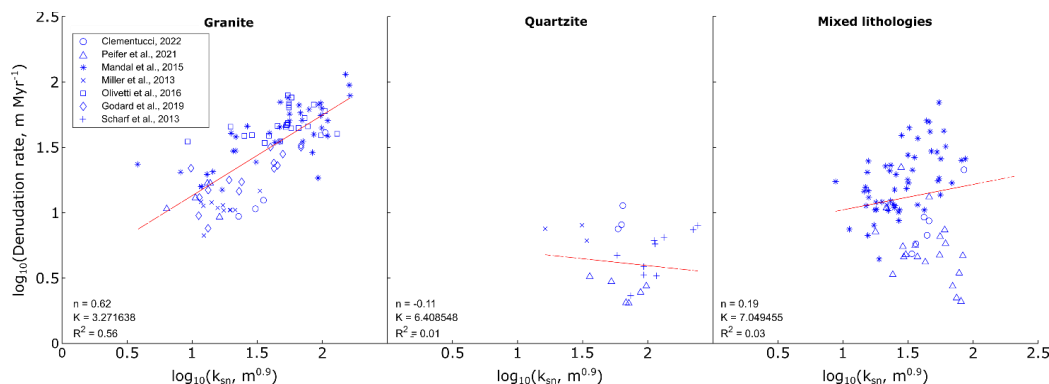


441
 442
 443
 444
 445
 446
 447

Figure 2. (a) Amount of eroded material for the performed experiments (the color coding follows Fig. 1); (b) Maximum incision rate as a function of the imposed boundary conditions; (c) Ae number computed for all the models; (d) Ae number plotted over the ratio between the imposed slope (S) and the applied rainfall rate (R).



448
 449 **Figure 3. a)** logarithm of the incision rate over the logarithm of the steepness index k_s for all the
 450 models. Imposed regional slope increases from top to bottom. Rainfall rate increases from left to
 451 right. Every plot shows four channels at every time step, forty channels total (colored dots). The
 452 linear regression is shown by the red line. Values related to the linear regression (n and K) are
 453 shown in the bottom right corner of every plot, together with the R^2 (units for K are $\text{mm}^{1-2m} \text{h}^{-1}$);
 454 **b)** same data of a), but plotted for every slope, without differentiating for rainfall rate.



456
 457 **Figure 4. Logarithm of the incision rate over the logarithm of the steepness index k_s for the**
 458 **selected natural prototypes. The linear regression is shown by the red line. Values related to the**
 459 **linear regression (n and K) are shown in every plot, together with the R^2 .**
 460
 461